Inorganic Chemistry
Article

Inorg. Chem. **2010**, *49*, 8465–8473 **8465**
DOI: 10.1021/ic101035q

Preparation, Size Control, Surface Deposition, and Catalytic Reactivity of Hydrophobic Corrolazine Nanoparticles in an Aqueous Environment

Kevin Cho,[†] William D. Kerber,[†] Se Ryeon Lee,[†] Albert Wan,[‡] James D. Batteas,*[,‡] and David P. Goldberg*[,†]

[†]*Department of Chemistry, Johns Hopkins University, 3400 N. Charles Street, Baltimore, Maryland 21218, and*
[‡]*Department of Chemistry, Texas A&M University, P.O. Box 30012, College Station, Texas 77842-3012*

Received May 21, 2010

Nanoparticles, each consisting of one of the three molecular corrolazine (Cz) compounds, $H_3(TBP_8Cz)$, $Mn^{III}(TBP_8Cz)$, and $Fe^{III}(TBP_8Cz)$ (TBP_8Cz = octakis(4-*tert*-butylphenyl)corrolazinato), were prepared via a facile mixed-solvent technique. The corrolazine nanoparticles (MCz-NPs) were formed in H_2O/THF (10:1) in the presence of a small amount of a polyethylene glycol derivative (TEG-ME) added as a stabilizer. This technique allows highly hydrophobic Czs to be "dissolved" in an aqueous environment as nanoparticles, which remain in solution for several months without visible precipitation. The MCz-NPs were characterized by UV−visible spectroscopy, dynamic light scattering (DLS), and transmission electron microscopy (TEM) imaging, and shown to be spherical particles from 100−600 nm in diameter with low polydispersity indices (PDI = 0.003−0.261). Particle size is strongly dependent on Cz concentration. The H_3Cz-NPs were adsorbed on to a modified self-assembled monolayer (SAM) surface and imaged by atomic force microscopy (AFM). Adsorption resulted in disassembly of the larger H_3Cz-NPs to smaller H_3Cz-NPs, whereby the resulting particle size can be controlled by the surface energy of the monolayer. The Fe^{III}Cz-NPs were shown to be competent catalysts for the oxidation of cyclohexene with either PFIB or H_2O_2 as external oxidant. The reactivity and product selectivity seen for Fe^{III}Cz-NPs differs dramatically from that seen for the molecular species in organic solvents, suggesting that both the nanoparticle structure and the aqueous conditions may contribute to significant changes in the mechanism of action of the Fe^{III}Cz catalyst.

Introduction

Porphyrins and their related analogues are desirable building blocks for nanomaterials because of their robust nature, their rich optical and redox properties, and their ability to house a wide variety of metal ions in their internal cavity. Given these promising characteristics, the preparation of porphyrinoid-based nanostructures has been a subject of intense interest, with catalytic, biological, and materials-related applications being targeted. For example, such applications include catalytic oxidations,[1,2] solar energy capture,[3−5] photoactive nanodevices,[6−8] dye aggregates,[9] and diagnostic[10] and therapeutic[11,12] agents. Porphyrinoid-based nanomaterials have been prepared via covalent and noncovalent assemblies that require specific interactions between molecular building blocks.[2,6,7,13] These assembly methods provide excellent control over the resulting architecture, but necessarily require careful design of the component molecules, and are intolerant to deviations in these components. Materials prepared by these methods include intricate nanostructures exhibiting a variety of morphologies, such as nanosheets,[8] nanotubes,[6] nanofibers,[14] and nanorods.[9,15−18]

*To whom correspondence should be addressed. E-mail: batteas@chem.tamu.edu (J.D.B.), dpg@jhu.edu (D.P.G.).

(1) Smeureanu, G.; Aggarwal, A.; Soll, C. E.; Arijeloye, J.; Malave, E.; Drain, C. M. *Chem.—Eur. J.* **2009**, *15*, 12133–12140.
(2) Drain, C. M.; Smeureanu, G.; Patel, S.; Gong, X. C.; Garno, J.; Arijeloye, J. *New J. Chem.* **2006**, *30*, 1834–1843.
(3) Yum, J. H.; Jang, S. R.; Humphry-Baker, R.; Grätzel, M.; Cid, J. J.; Torres, T.; Nazeeruddin, M. K. *Langmuir* **2008**, *24*, 5636–5640.
(4) Brumbach, M. T.; Boal, A. K.; Wheeler, D. R. *Langmuir* **2009**, *25*, 10685–10690.
(5) Ballesteros, B.; de la Torre, G.; Ehli, C.; Rahman, G. M. A.; Agullo-Rueda, F.; Guldi, D. M.; Torres, T. *J. Am. Chem. Soc.* **2007**, *129*, 5061–5068.
(6) Wang, Z. C.; Medforth, C. J.; Shelnutt, J. A. *J. Am. Chem. Soc.* **2004**, *126*, 16720–16721.
(7) Wang, Z. C.; Medforth, C. J.; Shelnutt, J. A. *J. Am. Chem. Soc.* **2004**, *126*, 15954–15955.
(8) Wang, Z. C.; Li, Z. Y.; Medforth, C. J.; Shelnutt, J. A. *J. Am. Chem. Soc.* **2007**, *129*, 2440–2441.
(9) Doan, S. C.; Shanmugham, S.; Aston, D. E.; McHale, J. L. *J. Am. Chem. Soc.* **2005**, *127*, 5885–5892.
(10) Duncan, T. V.; Ghoroghchian, P. P.; Rubtsov, I. V.; Hammer, D. A.; Therien, M. J. *J. Am. Chem. Soc.* **2008**, *130*, 9773–9784.
(11) McCarthy, J. R.; Perez, J. M.; Brückner, C.; Weissleder, R. *Nano Lett.* **2005**, *5*, 2552–2556.
(12) Brasseur, N.; Ouellet, R.; La Madeleine, C.; van Lier, J. E. *Br. J. Cancer* **1999**, *80*, 1533–1541.
(13) Drain, C. M.; Varotto, A.; Radivojevic, I. *Chem. Rev.* **2009**, *109*, 1630–1658.
(14) Wang, Z. C.; Ho, K. J.; Medforth, C. J.; Shelnutt, J. A. *Adv. Mater.* **2006**, *18*, 2557–2560.
(15) Schwab, A. D.; Smith, D. E.; Rich, C. S.; Young, E. R.; Smith, W. F.; de Paula, J. C. *J. Phys. Chem. B* **2003**, *107*, 11339–11345.
(16) Fuhrhop, J. H.; Bindig, U.; Siggel, U. *J. Am. Chem. Soc.* **1993**, *115*, 11036–11037.

Published on Web 08/25/2010

In contrast, non-specific methods of self-assembly, or more precisely "self-organization,"[13] of organic nanoparticles (ONPs) provide a potential alternative to the strict design requirements of self-assembly, albeit with reduced control over the exact architecture of the nanosized objects. One strategy for the self-organization of ONPs involves a rapid reduction in solubility of the desired organic molecular building blocks. This method usually involves the addition of a miscible nonsolvent (the "guest" solvent) to a solution (the "host" solvent) of the organic building block, causing the formation of a dispersion of ONPs in the guest solvent.[2,19−22] The resulting ONPs bear some similarities to colloidal materials, where their structures are dynamic in nature and held together by intermolecular interactions involving relatively weak forces (e.g., $\pi-\pi$ stacking, hydrophobic/hydrophilic effects). This mixed-solvent technique has been successfully employed by several research groups to prepare ONPs, and has been variously referred to as reprecipitation,[23] micronization,[20] or solvent-shifting.[19] A key advantage of the mixed-solvent procedure for making ONPs is that it can be applied to a wide range of molecular precursors, and it is not limited to specific bonding patterns or intermolecular interactions. Drain and co-workers have nicely adapted this method for the preparation of porphyrin-based ONPs, wherein nanoparticles based on either hydrophobic or hydrophilic porphyrins are easily prepared in aqueous or organic guest solvents, respectively.[2,22]

We have been involved with the development of a new class of porphyrinoid compounds known as corrolazines (Czs), which are formally hybrid molecules of the well-known ring-contracted corroles and the meso-*N*-substituted tetraazaporphyrins.[24,25] Corrolazines exhibit a range of novel properties and reactivity patterns that differ considerably from conventional porphyrins. Corrolazines, and their corrole analogs,[26−28] exhibit an unusual ability to stabilize high oxidation state metal ions, and facilitate subsequent oxidation chemistry and related atom- and group-transfer reactions such as epoxidations, hydroxylations, and aziridinations. To our knowledge, no reports of nanostructured materials based on corroles or corrolazines have appeared thus far. We thus set out to develop methods for preparing nanostructured materials based on these molecules, with the initial goal of using the Cz-based materials for catalytic applications. The mixed-solvent technique was selected for the formation of Cz-based nanoparticles because of its facile application, where the self-organization of the ONPs obviates the need for synthetic modification of the Cz macrocycle.

In addition to the interest in preparing porphyrinoid-based nanomaterials, there is also strong motivation to prepare porphyrinoid compounds that are water-soluble, in part because of the benefits of working in an inexpensive and environmentally friendly solvent. Significant efforts have been expended to synthesize water-soluble porphyrins[29−31] and corroles[32,33] but often the syntheses involve laborious, multistep procedures. We speculated that the mixed-solvent technique for ONP formation would provide a direct, one-step method for dispersing our hydrophobic corrolazines into water, providing us with water-soluble metallocorrolazines for "green catalysis" and other potential applications.

In this report we describe the preparation of nanoparticles from three different corrolazine building blocks, metal-free, iron(III), and manganese(III) corrolazine. The mixed-solvent technique has been employed to generate nanoparticles of controlled size and shape (spherical particles typically ∼200 nm in diameter). These corrolazine nanoparticles (Cz-NPs) are composed of highly hydrophobic corrolazines dispersed in aqueous solution, and have been characterized by UV−vis, dynamic light scattering (DLS), and transmission electron micrography (TEM) imaging. Particle size can be controlled by adjustment of the preparative conditions (concentration). To examine their stability on surfaces, Cz-NPs were also adsorbed on to modified SAM surfaces where the surface energy has been tuned by a controlled oxidative process.[34] The tuning of the surface energy dictates particle disassembly in a predictable fashion as observed by atomic force microscopy (AFM). The Fe^{III}Cz-NPs are shown to be catalytically active in the oxidation of cyclohexene with either iodosylarene or hydrogen peroxide as external oxidant. Examination of the catalytic behavior of the Fe^{III}Cz-NPs and comparison with that of the molecular Fe^{III}Cz in organic solvent reveals several important differences, including the ability to utilize H_2O_2 as external oxidant in the case of Fe^{III}Cz-NP with cyclohexene as substrate.

Experimental Section

General Procedures. All manipulations were performed under ambient conditions, and all reagents were used as received unless otherwise noted. Tetrahydrofuran (THF) was purchased from EMD Chemicals and purified by either a Pure Solv solvent purification system from Innovative Technologies, Inc., or distillation over Na/benzophenone under N_2(g). Octadecyltrichlorosilane (OTS) was purchased from Gelest, Inc. Si(100) substrates (double side polished) were purchased from University Wafer, Inc. Cu TEM grid and 2% uranyl acetate staining solution were purchased from Electron Microscopy Sciences and used as received. Water (R = 18.3 MΩ cm) was obtained using a Milli-Q Plus purification system from Millipore. Tri(ethylene glycol) monomethyl ether (TEG-Me), 4-bromo-1H-imidazole (4-Br-1H-Im), 1-methylimidazole, cyclohexene, 2-cyclohexen-1-ol and 2-cyclohexen-1-one were purchased from Sigma-Aldrich. 5-Chloro-1-methylimidazole (5-Cl-1-MeIm) was purchased from TCI America. Cyclohexene and decane

(17) Lee, S. J.; Malliakas, C. D.; Kanatzidis, M. G.; Hupp, J. T.; Nguyen, S. T. *Adv. Mater.* **2008**, *20*, 3543–3549.
(18) Wang, Z.; Lybarger, L. E.; Wang, W.; Medforth, C. J.; Miller, J. E.; Shelnutt, J. A. *Nanotechnology* **2008**, *19*, 395604.
(19) Brick, M. C.; Palmer, H. J.; Whitesides, T. H. *Langmuir* **2003**, *19*, 6367–6380.
(20) Horn, D.; Rieger, J. *Angew. Chem., Int. Ed.* **2001**, *40*, 4331–4361.
(21) Van Keuren, E.; Bone, A.; Ma, C. B. *Langmuir* **2008**, *24*, 6079–6084.
(22) Gong, X. C.; Milic, T.; Xu, C.; Batteas, J. D.; Drain, C. M. *J. Am. Chem. Soc.* **2002**, *124*, 14290–14291.
(23) Xiao, D. B.; Lu, X.; Yang, W. S.; Fu, H. B.; Shuai, Z. G.; Fang, Y.; Yao, J. N. *J. Am. Chem. Soc.* **2003**, *125*, 6740–6745.
(24) Kerber, W. D.; Goldberg, D. P. *J. Inorg. Biochem.* **2006**, *100*, 838–857.
(25) Goldberg, D. P. *Acc. Chem. Res.* **2007**, *40*, 626–634.
(26) Aviv-Harel, I.; Gross, Z. *Chem.—Eur. J.* **2009**, *15*, 8382–8394.
(27) Aviv, I.; Gross, Z. *Chem. Commun.* **2007**, 1987–99.
(28) Gryko, D. T.; Fox, J. P.; Goldberg, D. P. *J. Porphyrins Phthalocyanines* **2004**, *8*, 1091–1105.
(29) Ikawa, Y.; Harada, H.; Toganoh, M.; Furuta, H. *Bioorg. Med. Chem. Lett.* **2009**, *19*, 2448–2452.
(30) Manono, J.; Marzilli, P. A.; Fronczek, F. R.; Marzilli, L. G. *Inorg. Chem.* **2009**, *48*, 5626–5635.
(31) Cao, Y.; Gill, A. F.; Dixon, D. W. *Tetrahedron Lett.* **2009**, *50*, 4358–4360.
(32) Gross, Z.; Galili, N.; Saltsman, I. *Angew. Chem., Int. Ed.* **1999**, *38*, 1427–1429.
(33) Gershman, Z.; Goldberg, I.; Gross, Z. *Angew. Chem., Int. Ed.* **2007**, *46*, 4320–4324.
(34) Roberson, S. V.; Fahey, A. J.; Sehgal, A.; Karim, A. *Appl. Surf. Sci.* **2002**, *200*, 150–164.

were purchased from Fluka. Pyridine was purchased from Fisher Scientific and used as received. 30% H_2O_2 was purchased from J.T. Baker. Pentafluoroiodosylbenzene (PFIB),[35] $Mn^{III}(TBP_8Cz)$[36] (TBP_8Cz = octakis(4-*tert*-butylphenyl)corrolazinato), $Fe^{III}(TBP_8Cz)$,[37] and $H_3(TBP_8Cz)$[38] were synthesized according to the literature.

Instrumentation. UV−vis spectroscopy was performed on an Agilent 8453 spectrometer. DLS data were obtained by a Zetasizer Nano ZS90 (Malvern Instruments) fitted with a 633 nm laser. The parameters for the dispersant were a viscosity of 0.9080 cP and an index of refraction of 1.34. Samples for TEM were prepared by absorption of nanoparticles on to a Cu TEM grid followed by staining with 2% uranyl acetate. The TEM images were obtained by an FEI Tecnai 12 TWIN transmission electron microscope equipped with a SIS Megaview III Wide-angle camera. The AFM images were obtained in tapping mode with a WiTec alpha300 S under ambient conditions. Gas chromatography (GC) was performed on an Agilent 6850 gas chromatograph fitted with a DB-5 5% phenylmethyl siloxane capillary column (30 m × 0.32 mm × 0.25 μm) and equipped with a flame ionization detector. GC-FID response factors for cyclohexene oxide, 2-cyclohexen-1-ol, and 2-cyclohexen-1-one were prepared versus decane as an internal standard.

Preparation of M(TBP_8Cz) (M = Mn, Fe, H_3) Nanoparticles. In a typical preparation, 50 μL of a stock solution of M(TBP_8Cz) in THF (1.6 mM) was transferred to a 20 mL vial and diluted with 450 μL of THF to give a final concentration of 0.16 mM of corrolazine. To this solution was added TEG-Me (50 μL), and this mixture was stirred slowly for 5 min to ensure homogeneity. While stirring at the same rate, Milli-Q H_2O (5.0 mL) was added slowly dropwise (1−2 min for complete addition) giving a final solution composed of H_2O/THF (10:1). Care must be taken to keep the stirring rate of the mixture slow and constant throughout the addition of H_2O to prevent precipitation of the corrolazine. After the addition of H_2O is complete, it is important to stir the nascent nanoparticles for an additional 1−5 min until the solution is completely homogeneous. The final nanoparticle solution appears translucent with no precipitates.

Preparation of SAMs with Tunable Surface Energies. A 10 mm × 20 mm piece of silicon wafer was first oxidized in a mixture of 12 mL H_2O, 3 mL of 30% H_2O_2 and 3 mL concentrated NH_4OH at 85 °C for 40 min, and then cleaned with copious amounts of water and dried under a jet of streaming nitrogen. The cleaned and oxidized Si wafer was then immersed in a 0.25 mM of OTS/hexanes solution with sonification at room temperature for 2 h. The sample was then washed in THF, water, ethanol, and dried with N_2 and then characterized by infrared spectroscopy (Thermo Nicolet 6700 FTIR) and static water contact angle measurements. The infrared spectrum showed the appearance of C−H symmetric stretching frequency at 2852 cm^{-1} and C−H asymmetric stretching frequency at 2918 cm^{-1}. The OTS surface exhibited a static water contact angle of ∼110°. The C−H asymmetric stretch of 2918 cm^{-1} is indicative of a well ordered OTS monolayer, which is consistent with the large water contact angle. A gradient in surface energy was prepared on the Si wafer by selectively oxidizing the OTS monolayer to varying degrees using an ultraviolet/ozone gradient instrument. This home-built instrument consists of a UV-lamp with emission wavelengths of 254 and 285 nm, which was used to produce ozone and oxidize the surfaces. The OTS coated Si wafer is rastered underneath the UV lamp at a distance of about 1 mm with a computer controlled micropositioning stage (Zaber Technologies Inc., Canada). The wafer was divided evenly into four 5 × 10 mm^2 regions using a diamond cut to mark their boundaries. The sample was placed on the scan stage and moved under the UV-lamp at a constant rate of 0.032 mm/s and each region of the OTS/Si wafer was exposed to the UV light 10 sweeps, 6 sweeps, 2 sweep, with the last region receiving no exposure to produce the surface energy gradient with static water contact angle of 40°, 60°, 75°, and 110°, respectively for each region. All 4 regions were scanned using AFM tapping mode to confirm there were no cluster-like species on the surface before depositing $H_3(TBP_8Cz)$ nanoparticles.

Deposition and AFM Characterization of Nanoparticles. $H_3(TBP_8Cz)$ nanoparticles were deposited on the surface energy gradient by drop-casting 5 μL of the diluted (1600:1) $H_3(TBP_8Cz)$ nanoparticles suspension on each region which were then air-dried in a covered Petri dish. AFM images of the deposited nanoparticles were collected on the central regions of the dried droplet areas.

Catalytic Oxidation of Cyclohexene. In a typical catalytic reaction, nanoparticles of $Fe^{III}(TBP_8Cz)$ (0.11 mM) were freshly prepared in 2.35 mL of H_2O/THF (10:1) as described above. In reactions with PFIB as the oxidant, cyclohexene (30 μL, 110 mM) was added dropwise to the FeCz-NP solution and mixed for 5 min, and then PFIB (13.6 mg, 22 mM) was added as a solid to this mixture. The reaction mixture was stirred at 298 K until complete bleaching of the catalyst was noted (∼4 h). When H_2O_2 was used as the oxidant, a nitrogenous base (5-Cl-1-MeIm, 1-MeIm, pyridine, or 4-Br-1H-Im) (2.75 mM) was added dropwise to the Fe^{III}Cz-NP solution, followed by the dropwise addition of cyclohexene (15 μL,56 mM). After mixing for 5 min, the reaction was initiated by the dropwise addition of 30% H_2O_2 solution (6.4 μL, 22 mM). The reaction mixture was stirred at 298 K until complete bleaching of the catalyst was noted (20−24 h). The reaction mixture was extracted with CH_2Cl_2 (2 × 0.5 mL) and *n*-decane was added to the organic layer. The CH_2Cl_2 layer was then injected directly on the GC for product analysis. GC retention times: *n*-decane 4.5 min, cyclohexene oxide 2.9 min, 2-cyclohexen-1-ol 3.3 min, and 2-cyclohexen-1-one 3.8 min. All catalytic runs were performed at least in triplicate. GC-FID conditions for cyclohexene oxidation products: An initial oven temperature of 70 °C was held for 3 min and then raised 40 °C/min until a temperature of 100 °C was reached. This temperature was held for 7 min.

Results and Discussion

Formation of Nanoparticles. The basic protocol for formation of the corrolazine nanoparticles is shown in Scheme 1. In this protocol, a hydrophobic corrolazine M(TBP_8Cz) (M = H_3, Mn, Fe) was dissolved in an appropriate amount of the water-miscible organic solvent tetrahydrofuran (THF), and mixed with a small amount of a polyethylene glycol-derived stabilizer (e.g., TEG-Me). The organic solution and the stabilizer are mixed for just enough time so as to make sure the resulting solutions are homogeneous. The critical step in the nanoparticle formation takes place upon addition of water to the organic Cz solution. It is essential that water is added dropwise, with *slow mixing* by a magnetic stir bar or agitating the organic solution on an automated rocker. The nanoparticles will not form if the solution is mixed too vigorously, or not mixed at all, during H_2O addition, and instead immediate precipitation of the corrolazine will occur. This preparation contrasts that used for other

(35) McGown, A. J.; Kerber, W. D.; Fujii, H.; Goldberg, D. P. *J. Am. Chem. Soc.* **2009**, *131*, 8040–8048.
(36) Lansky, D. E.; Mandimutsira, B.; Ramdhanie, B.; Clausén, M.; Penner-Hahn, J.; Zvyagin, S. A.; Telser, J.; Krzystek, J.; Zhan, R. Q.; Ou, Z. P.; Kadish, K. M.; Zakharov, L.; Rheingold, A. L.; Goldberg, D. P. *Inorg. Chem.* **2005**, *44*, 4485–4498.
(37) Kerber, W. D.; Ramdhanie, B.; Goldberg, D. P. *Angew. Chem., Int. Ed.* **2007**, *46*, 3718–3721.
(38) Ramdhanie, B.; Stern, C. L.; Goldberg, D. P. *J. Am. Chem. Soc.* **2001**, *123*, 9447–9448.

Scheme 1

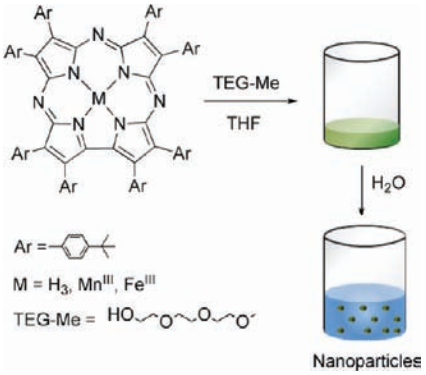

metalloporphyrins, in which vigorous mixing (e.g., sonication) and rapid addition of the aqueous phase was employed.[1,2,22] The stark contrast in methods of mixing for the MCz-NP formation, as opposed to the earlier metalloporphyrin methods, may be attributed to the significantly more hydrophobic nature of the Cz macrocycle. The Cz ligand contains eight peripheral aryl substituents, whereas metalloporphyrins employed previously for ONP formation contained at most four hydrophobic aryl groups.[2,22] It was also noted that constant mixing of the MCz-NP solutions for long periods after the addition of H_2O is complete induced precipitation of the nanoparticles, and thus mixing was generally stopped after H_2O addition.

Successful preparation of the MCz-NPs results in the formation of a green or yellow translucent solution with no visible solid particulates. Solutions of NPs derived from metal-free, iron(III), and manganese(III) Cz's and prepared under relatively dilute conditions (10−50 μM) are highly stable, remaining in solution for several months at ambient conditions on the benchtop. Decomposition of the NPs is characterized by precipitation of the corrolazines from solution, which is easily visible to the naked eye. Solutions of MCz-NPs could be prepared with effective higher concentrations (50−300 μM) of corrolazine, although in these cases somewhat lower stability was observed. For example, both the Mn^{III}Cz-NPs and Fe^{III}Cz-NPs stayed in solution for ~1 week at concentrations up to 150 μM, but at ~300 μM precipitation was noted after aging for 2 days on the benchtop. Interestingly, attempts to redissolve precipitated MCz-NPs by vigorous stirring or shaking of the solutions failed, but sonication of the mother liquor did result in redissolution of the nanoparticles. However, MCz-NPs redissolved by the sonication process showed limited stability, and typically precipitated again after ~24 h.

UV−vis Spectroscopy. The UV−vis spectra of Mn^{III}-(TBP_8Cz), H_3(TBP_8Cz), and Fe^{III}(TBP_8Cz) nanoparticles, together with the parent spectra of the different corrolazines are shown in Figure 1. As seen in Figure 1a, the parent spectrum of Mn^{III}(TBP_8Cz) in pure THF has an intense Soret band at 437 nm with a smaller peak at 496 nm, and a Q-band at 693 nm with smaller features at 565 and 635 nm. This spectrum is typical of a metallocorrolazine, with $\pi-\pi^*$ macrocyclic transitions dominating the spectrum. Upon formation of the nanoparticles, there is a significant decrease in intensity and apparent broadening of the Soret band, along with the appearance of an additional maximum at 469 nm. The Q-band also decreases in intensity at 693 nm, but no obvious broadening is observed. The smaller features at 565 and 635 also appear somewhat broadened. The spectrum of the metal-free corrolazine, shown in Figure 1b, shows similar changes upon conversion of the molecular corrolazines in THF to nanoparticles in aqueous media. In this case, both the Soret (460 nm) and Q-band (678 nm) lose intensity and show significant broadening upon NP formation. In contrast to the Mn^{III}Cz-NPs, there is a slight red-shift of ~3 nm in the Soret band, and a more dramatic blue-shift of the Q-band of 11 nm. The Fe complex also shows a decrease and apparent broadening of the major features of the UV−vis spectrum upon NP formation, as seen in Figure 1c. For all three complexes, the absorption spectra of the nanoparticles appear to follow Beer's law. As shown in Figure 1d, there is a smooth decrease of the Mn^{III}Cz-NP absorbance upon dilution of the nanoparticles by addition of increasing amounts of water. Plots of absorbance at 437, 469, or 693 nm versus effective concentration of Mn(III) complex (i.e., total moles of Mn(III) complex/solution volume) for the Mn^{III}Cz-NP solutions show good linear correlations (Supporting Information, Figures S1−S3). Similar linear correlations are seen for dilution experiments with both H_3Cz- and Fe^{III}Cz-NPs (Supporting Information, Figures S4−S5).

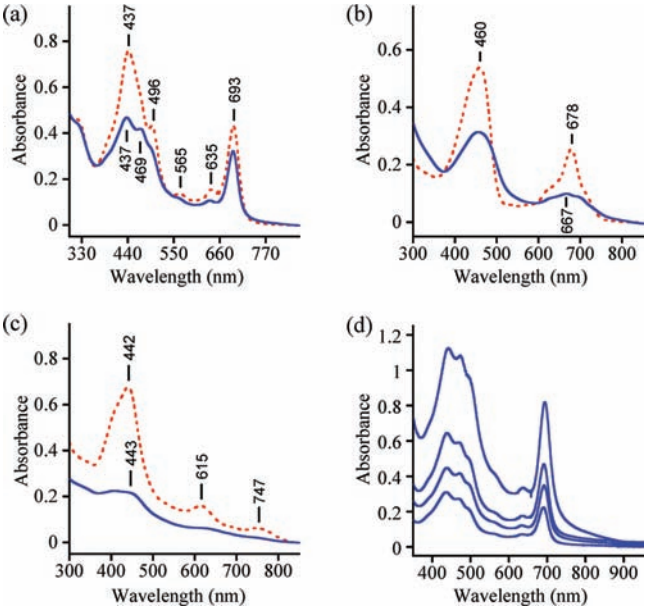

Figure 1. UV−vis spectra of molecular corrolazine in neat THF (dashed red line) and its corresponding nanoparticles in H_2O/THF (10:1) (solid blue line) for (a) Mn^{III}Cz (14 μM) (b) H_3Cz (56 μM), and (c) Fe^{III}Cz (14 μM) and (d) Mn^{III}Cz-NP in H_2O/THF (10:1) over the concentration range 7.2−57.6 μM.

The loss in intensity and broadening of the peaks observed for the Cz compounds in Figure 1 are characteristic of the formation of porphyrinoid nanoparticles.[22] Nanoparticles prepared by using the same mixed-solvent technique with hydrophobic porphyrins (e.g., tetraphenylporphyrin) exhibited the same dramatic broadening for both the Soret and Q-band features.[21,22] The phthalocyanine (Pc) macrocycle may be considered a closer structural analogue of a corrolazine because of the bridging *meso*-N atoms. Typically, the UV−vis spectra of Pc's

match more closely to Cz spectra, with Q-bands considerably more intense than Q-bands for porphyrins.[39] A recent study involving the conversion of magnesium phthalocyanine (MgPc) to water-soluble nanoparticles via the mixed-solvent technique (host solvent = acetone; guest solvent = water) showed that the Q-band decreased significantly in intensity upon conversion of molecular MgPc to nanoparticle.[21] Interestingly, this decrease was not accompanied by a dramatic broadening as seen for the porphyrins, but more closely resembled the decrease observed for Mn^{III}Cz-NPs (Figure 1a).

Previously, certain features of the UV−vis spectra of porphyrin nanoparticles[22] and related organic aggregates have been used as markers for structural arrangements of the molecular building blocks.[20,40−42] A blue-shift of the Soret band for porphyrins arises from the so-called H-aggregate ("face-to-face") structure, and a red-shift can be attributed to a J-aggregate ("edge-to-edge") structure. For the MCz-NPs, the Mn(III) complex exhibits a splitting in the Soret band upon NP formation. This apparent splitting, caused by the appearance of a second red-shifted peak at 469 nm, suggests J-aggregate structural components within the Mn^{III}Cz-NPs, as seen for tetrakis(4-sulfonatophenyl)porphyrin.[40,41] The metal-free and iron(III) corrolazines do not show any obvious shift in the Soret region that would support assignment of H- and J-aggregates, suggesting that these particles may contain both types of structural components or lack long-range ordering of this type.

DLS Spectroscopy and TEM Imaging. DLS was employed for measurements of nanoparticle size in solution for the MCz-NPs. Typical size distribution plots for the three types of nanoparticles are shown in Figure 2 and the data are summarized in the Supporting Information, Table S1. The data are displayed as histograms showing the percentage of particles versus hydrodynamic diameter. The average diameter of the Mn^{III}Cz-NPs in Figure 2a is 230 nm with a polydispersity index (PDI)[21] of 0.138. The iron(III) and metal-free nanoparticles (Figures 2b−c) are of similar size, with average diameters of 168 and 181 nm, respectively, and are also relatively monodisperse. DLS measurements on different batches of each of the three corrolazine nanoparticles showed good reproducibility, with the average diameter varying at most by ∼25% and PDI values <0.25. These data suggest that the rate of mixing and rate of water addition during the nanoparticle formation, which are the variables most difficult to control, do not have a large influence over particle size and distribution. However, particle size for the MCz-NPs does depend strongly on the total concentration of corrolazine. As shown in Figure 2d, the average diameter more than doubles at the highest concentrations while the polydispersity remains relatively narrow (Supporting Information, Table S1). Thus the DLS data show that the mixed-solvent method

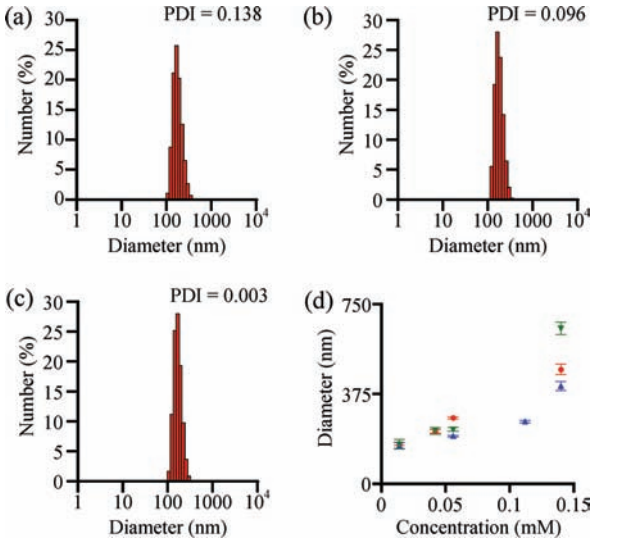

Figure 2. Representative DLS histograms and PDI for (a) Mn^{III}Cz-NP (14.4 μM), (b) H_3Cz-NP (14.4 μM), and (c) Fe^{III}Cz-NP (14.4 μM) and (d) dependence of average diameter on concentration for H_3Cz-NP (solid green downward-pointed triangles), Mn^{III}Cz-NP (solid red circles), and Fe^{III}Cz-NP (solid blue upward-pointed triangles).

for preparing MCz-NPs allows for good size control with low polydispersity for the resulting nanoparticles.

In comparison, nanoparticles prepared from MgPc via the same mixed-solvent procedure fall into a similar size regime (100−500 nm). However, the average particle size for MgPc depended strongly on solvent ratios, and were also influenced by inexact mixing methods.[21] In contrast, porphyrin-based nanoparticles seem to favor a smaller size regime (∼20−200 nm), with the size dependent on the nature of the molecular porphyrin.[2,22] For the porphyrin derivative $TPPF_{20}$, it was shown that at low concentrations (<10 μM) of the molecular porphyrin the resulting nanoparticle size decreased significantly, but then exhibited a modest increase in diameter up to 40 μM.[2,22] These results are different than for our MCz-NPs, which show dramatic increases in diameter upon increasing MCz concentration.

Further characterization of the MCz-NPs was carried out by TEM. Representative images are shown in Figure 3 for the three MCz-NPs adsorbed on Cu-TEM grids and stained with uranyl acetate. The three types of nanoparticles clearly exhibit an approximate spherical morphology. Diameter measurements from TEM on a number of nanoparticles are in good agreement with the sizes measured by DLS for the respective MCz-NPs (100−300 nm). Given the dynamic nature of the MCz-NPs in solution, one would predict that the size and morphology of these particles could be perturbed by adsorption on to the TEM grid, but the data indicate that the particles remain intact under the conditions of the TEM imaging experiments. These data help confirm the spherical nature of the particles in solution, which is important for the DLS analysis because it relies upon the assumption that the NPs behave as hard spheres in solution. It is satisfying to see that the size and shape of the MCz-NPs in Figure 3 are in excellent agreement with the DLS data.

AFM Studies. To examine the influence of the surface interaction on the morphology of MCz-NPs, the H_3-(TBP_8Cz) nanoparticle suspensions were deposited on a surface energy gradient prepared by oxidizing an OTS-Si

(39) Kadish, K. M., Smith, K. M., Guilard, R. *The Porphyrin Handbook*; Academic Press: San Diego, CA, 2003; Vols. *15*−*20*.
(40) Maiti, N. C.; Mazumdar, S.; Periasamy, N. *J. Porphyrins Phthalocyanines* **1998**, *2*, 369–376.
(41) Maiti, N. C.; Mazumdar, S.; Periasamy, N. *J. Phys. Chem. B* **1998**, *102*, 1528–1538.
(42) Xu, W.; Guo, H. Q.; Akins, D. L. *J. Phys. Chem. B* **2001**, *105*, 1543–1546.

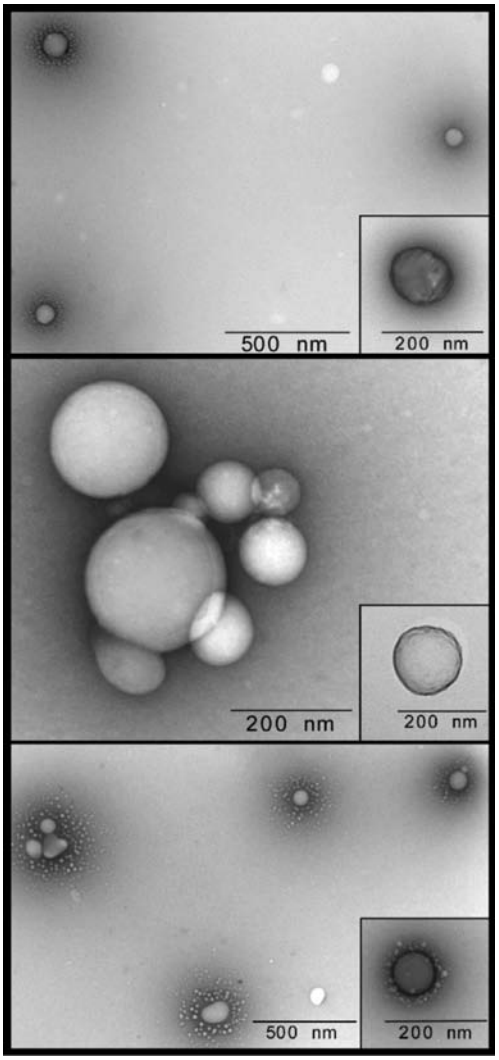

Figure 3. TEM images of (top) Mn^{III}Cz-NP (middle) H_3Cz-NP and (bottom) Fe^{III}Cz-NP. Insets: best view of an isolated MCz-NP.

SAM surface with UV light, and then characterized by AFM imaging in tapping mode. Oxidizing OTS with UV light produces carboxyl species,[34] thus lowering the water contact angle of the surface and increasing the surface hydrophilicity. An illustration depicting the process of oxidizing the OTS-Si SAM surface and the disassembly of the H_3Cz-NPs onto the treated surface can be seen in Figure 4. Figure 5 shows the AFM images and the size distribution of $H_3(TBP_8Cz)$ nanoparticles on OTS-Si substrate with various contact angles. On the clean OTS surface with contact angle 110° (no UV light exposure), the average size of the nanoparticles is 227 ± 65 nm (Figure 5a and e). This is similar to the size obtained by DLS and TEM. Therefore, it is likely the nanoparticles maintained their solution phase morphologies on the hydrophobic OTS modified Si surface. On the surface with contact angle 75°, the average size of the nanoparticles decreases to 42 ± 27 nm (Figure 5b and f). The particle size decreases to 11 ± 3 nm and 13 ± 4 on the surfaces with contact angle of 60° (Figure 5c and g) and 40° (Figure 5d and h), respectively. Occasionally, on the surfaces with contact angle of ~60°, collapse of the large nanoparticles was observed in some regions (Supporting Information, Figure S6). These data indicate that interfaces with high surface energies favor the disassembly of $H_3(TBP_8Cz)$ nanoparticles, producing small nanoparticles of about 10−15 nm with a relatively uniform size distribution. Figure 6 shows how the average particle size varies with the contact angle of the modified OTS-Si surface. A similar breakdown process has been reported for porphyrin ONPs.[2,22]

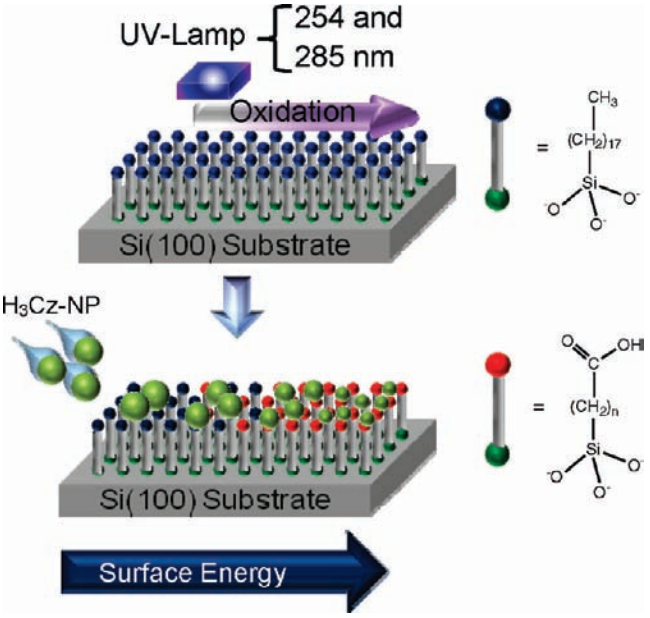

Figure 4. Illustration depicting the treatment of the OTS/Si SAM surface by sweeping under a UV-lamp (top) and the adsorption and disassembly of H_3Cz-NPs on to regions of the surface with varying degrees of oxidation of the SAM (bottom).

Catalysis. Earlier work from our group showed that $Fe^{III}(TBP_8Cz)$ functioned as a catalyst in the oxidation of either thioethers or alkenes.[35] The external oxidants employed in the oxidation of alkenes were iodosylarenes (PhIO or PFIB), and H_2O_2 was used for the oxidation of thioethers. For example, oxidation of cyclohexene with PFIB resulted in rapid turnover and high selectivity for cyclohexene oxide. Oxidation of other alkene substrates, such as styrene or cyclooctene, also showed rapid turnover with PFIB, although the selectivity was not as high for epoxide in the case of styrene. Evidence was presented for the formation of a high-valent iron-oxo species as the catalytically active intermediate. We desired to replace PFIB with the more economical and environmentally friendly oxidant H_2O_2.[43] Attempts to use H_2O_2 as oxidant led to efficient and selective oxidation of thioether substrates to sulfoxide, but failed to give any oxidation products with alkene substrates, suggesting that a high-valent iron-oxo species did not form in this case.[37] With the successful preparation of water-soluble corrolazine nanoparticles, we sought to test the catalytic behavior of these particles and compare them to the molecular species.

(43) For recent examples of work where both iodosylarenes and H_2O_2 were employed as external oxidants in related iron phthalocyanine oxidation catalysis, see: (a) Sorokin, A. B.; Kudrik, E. V.; Bouchu, D. *Chem. Commun.* **2008**, 2562–2564. (b) Geraskin, I. M.; Pavlova, O.; Neu, H. M.; Yusubov, M. S.; Nemykin, V. N.; Zhdankin, V. V. *Adv. Synth. Catal.* **2009**, *351*, 733–737. (c) Geraskin, I. M.; Luedtke, M. W.; Neu, H. M.; Nemykin, V. N.; Zhdankin, V. V. *Tetrahedron Lett.* **2008**, *49*, 7410–7412. (d) Neu, H. M.; Yusubov, M. S.; Zhdankin, V. V.; Nemykin, V. N. *Adv. Synth. Catal.* **2009**, *351*, 3168–3174.

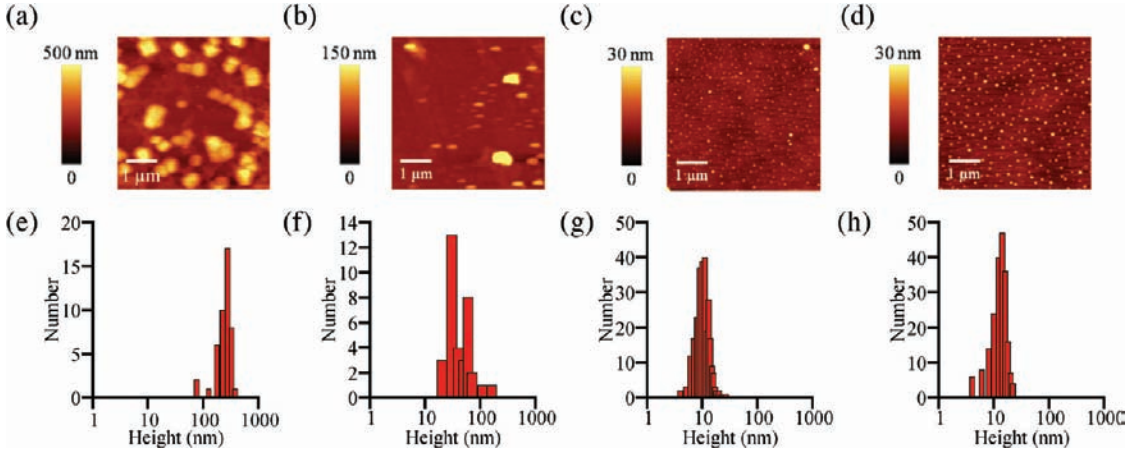

Figure 5. Topographic AFM images and size distribution of H_3Cz-NPs adsorbed on to UV/ozone-treated OTS-Si substrate. (a), (b), (c), and (d) are the AFM images of H_3Cz-NPs adsorbed on OTS-Si with contact angle 110°, 75°, 60°, and 40°, respectively. (e), (f), (g), and (h) are the size distribution of H_3Cz-NPs adsorbed on OTS-Si with contact angle 110°, 75°, 60°, and 40°, respectively.

Table 1. Oxidation Of Cyclohexene Catalyzed By $Fe^{III}(TBP_8Cz)$ and $Fe^{III}Cz$-NP

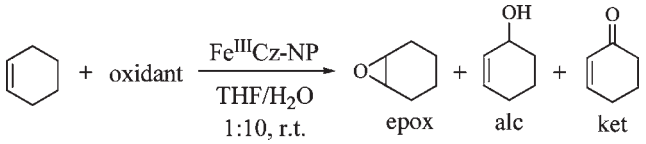

entry	catalyst	[$Fe^{III}Cz$] (μM)	size[a] (nm)	oxidant	additive	epox[b] (%)	alc[b] (%)	ket[b] (%)	yield[b,c] (%)	TON[d]
1[e]	$Fe^{III}Cz$	0.7		PFIB		33	2	2	37	37
2[f]	$Fe^{III}Cz$-NP	14	159	PFIB		5	11	21	37	37
3[f]	$Fe^{III}Cz$-NP	56	199	H_2O_2	5-Cl-1-MeIm[g]	6	5	13	24	24
4[f]	$Fe^{III}Cz$-NP	56	199	H_2O_2	1-MeIm[g]	3	<1	6	10	10
5[h]	$Fe^{III}Cz$-NP	110	259	H_2O_2	5-Cl-1-MeIm[g]	16	18	48	82	164
6[h]	$Fe^{III}Cz$-NP	110	259	PFIB		<1	49	47	99	199
7[i]	$Fe^{III}Cz$-NP	110	259	H_2O_2	5-Cl-1-MeIm[g]	8	3	10	21[j]	210

[a] Average diameter based on DLS data. [b] Determined by GC. [c] Percent yield = (mols of epox + alc + ket)/(mols of oxid) × 100, unless otherwise noted. [d] Turnover number (TON) = (mols of epox + alc + ket)/(moles of $Fe^{III}Cz$). [e] Molecular $Fe^{III}Cz$/PFIB/cyclohexene (1:100:1000) in CH_2Cl_2:MeOH (3:1 v:v). ref 35. [f] Catalyst/oxidant/substrate = 1:100:1000. [g] [additive] = 25 × [$Fe^{III}Cz$]. [h] Catalyst/oxidant/substrate = 1:200:500. [i] Catalyst/oxidant/substrate = 1:2000:1000. [j] Percent yield = (mols of epox + alc + ket)/(mols of cyclohexene) × 100.

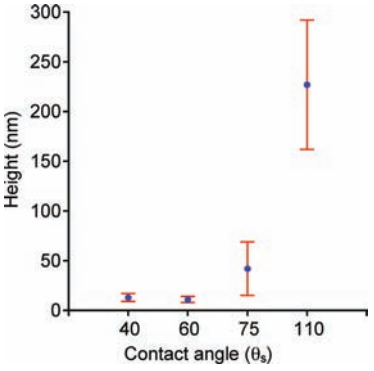

Figure 6. Average height of H_3Cz-NPs versus the contact angle of the OTS modified Si surface. With increasing surface energy, the nanoparticle size decreases down to about 10 nm.

Initial catalysis studies were made with the iron(III) nanoparticles as catalyst, PFIB as external oxidant, and cyclohexene as substrate (Table 1). The reaction was initiated by addition of PFIB to an aqueous suspension of the substrate and $Fe^{III}Cz$-NPs, and was run until complete degradation of the nanoparticles was noted by the formation of clear, colorless solutions. As shown in Table 1 (entry 2), three oxidation products, cyclohexene oxide, 2-cyclohexen-1-ol, and 2-cyclohexen-1-one were formed, giving an overall turnover number (TON) of 37 on a per corrolazine basis. The TON is in close agreement with that seen for the molecular $Fe^{III}(TBP_8Cz)$ (entry 1), although the reaction times were significantly longer for the $Fe^{III}Cz$-NPs, typically taking 4 h for complete degradation of the catalyst as compared to 2 min for the same reaction with the molecular $Fe^{III}(TBP_8Cz)$. In addition, the product ratios were dramatically different, with a 1:2:4 ratio for oxide/alcohol/ketone observed for the nanoparticle catalyst, as compared to a 16:1:1 ratio for the molecular species. The longer reaction times seen for the nanoparticles may in part be due to the more limited solubility of the oxidant PFIB in aqueous solution as compared to the CH_2Cl_2/MeOH mixture employed for the reaction with the molecular metallocorrolazine. Previous work has shown that similar organic nanoparticles constructed from metalloporphyrins also exhibit significantly slower reaction rates compared to the molecular metalloporphyrins for catalytic oxidations.[1] The large shift in product ratios for the $Fe^{III}Cz$-NPs possibly reflects steric effects induced by the nanoparticle environment on the approach of the cyclohexene substrate.

The initial work with PFIB established that the Fe^{III}Cz-NPs could function as oxidation catalysts with reasonable TONs and good stability. The PFIB was then replaced by 30% H_2O_2 as the external oxidant, but only trace oxidation products of cyclohexene were observed by GC along with complete bleaching of the catalyst. These results were similar to our previous findings, where no oxidation of cyclooctene was seen with H_2O_2 as oxidant and molecular Fe^{III}Cz as catalyst in organic solvent.[37] We then varied the pH of the Fe^{III}Cz-NP/H_2O_2 reaction, speculating that a possible iron-(hydro)peroxo adduct may be activated to give a high-valent iron-oxo species under either basic or acidic conditions. Both base- or acid-induced O−O bond cleavage in Fe-OO(H) porphyrin adducts has been shown to give oxidatively reactive, high-valent iron-oxo species.[44,45] The Fe^{III}Cz-NP solutions were stable over a wide range of pH (2−11) and different buffers (acetate, formate, borate), but at no pH was the catalytic oxidation of cyclohexene observed.

With the molecular $Fe^{III}(TBP_8Cz)$ as catalyst, it was found that the addition of the axial donor ligand *N*,*N*-(dimethylamino)pyridine (DMAP) enhanced the reactivity with H_2O_2 in the oxidation of thioethers.[37] Thus we attempted the addition of exogenous bases as potential axial donors for the iron nanoparticles, with the intent of activating H_2O_2 for alkene oxidation. We were pleased to find that the addition of 5-Cl-1-MeIm resulted in the formation of significant yields of cyclohexene oxidation products with Fe^{III}Cz-NPs as catalyst and H_2O_2 as oxidant (Table 1, entry 3). The major product is the ketone, as seen for the Fe^{III}Cz-NP/PFIB reaction. In contrast, the addition of 5-Cl-1-MeIm to the molecular $Fe^{III}(TBP_8Cz)$ in neat THF yielded only negligible amounts of the three cyclohexene oxidation products with H_2O_2 as oxidant. Thus the formation of NPs in H_2O, combined with the proper heterocyclic base, allows for the use of H_2O_2 as oxidant in the oxidation of cyclohexene. The organization of the iron corrolazines within the nanoparticles is not known, and is likely to be dynamic in nature. It is difficult to determine the number of iron sites accessible to the nitrogenous bases, but the dynamic nature of the NPs make it likely that at least some of the iron sites both on the surface and within the nanoparticles are available for coordination by axial donors and interaction with substrates.

A dramatic improvement in TON for the H_2O_2 reactions was made by increasing the catalyst concentration (entry 3 vs 5) and modifying the ratios of catalyst:substrate/oxidant (entry 3 1:100:1000, entry 5 1:200:500). Reexamination of the PFIB reaction under the same conditions of increased catalyst concentration also results in a significant increase in TON (entry 6). Addition of a large excess of H_2O_2 versus substrate leads to a modest increase in TON (entry 7 versus entry 5), but significantly lower overall yield.

We also examined the same reactions with PFIB or H_2O_2 under anaerobic conditions, and found no significant change in product yield, distribution, or TON. Although the observation of ketone as the dominant product is consistent with an autoxidation mechanism,[46,47] the results under anaerobic conditions argue against an autoxidation pathway. In addition, similar reactions were performed with pure O_2 or air in place of H_2O_2, and no oxidation products were observed. Further work is needed to obtain more detailed mechanistic insights.

Addition of 1-MeIm instead of 5-Cl-1-MeIm to the Fe^{III}Cz-NP/H_2O_2 system does help facilitate the oxidation of cyclohexene, but the yields are significantly lower (entry 4). Addition of other nitrogenous bases such as 4-Br-1H-Im or pyridine failed to give any catalytic activity toward cyclohexene, and only the typical, slow bleaching of the Fe^{III}Cz-NP is observed. A similar dependence on exogenous bases has been noted for oxidations of alkenes catalyzed by aqueous porphyrins and H_2O_2.[44,45] In one study, the same advantage was noted for using 5-Cl-1-MeIm over 1-MeIm to give the best yield of epoxide in the oxidation of alkenes by Fe(TPPF$_{20}$)/H_2O_2.[44] The reactivity of the Fe^{III}Cz-NP/H_2O_2 system is clearly influenced by the identity of the nitrogenous base, with 5-Cl-1-MeIm providing by far the best yields and TON in the oxidation of cyclohexene.

Conclusions

Water-soluble, organic nanoparticles from highly hydrophobic corrolazines have been prepared by a simple and convenient mixed-solvent technique, and characterized by UV−vis, DLS, TEM, and AFM measurements. This method provides spherical nanoparticles that are relatively monodisperse in size, and these ONPs can remain stable and soluble for several months under ambient conditions. In addition, the size of the ONPs can be easily controlled by either adjusting concentration of the molecular starting material or depositing onto OTS-modified silicon surfaces of controlled surface energies. These results are consistent with the presumed dynamic nature of the ONPs, which are assembled by relatively weak intermolecular forces. Their dynamic nature is advantageous in that different particle sizes can be accessed easily in solution or on the OTS modified Si surface.

The iron corrolazine-based nanoparticles were tested for their ability to catalyze the oxidation of cyclohexene. With PFIB as external oxidant, the Fe^{III}Cz-NPs exhibit good catalytic activity with similar TON as seen for the molecular catalyst under similar conditions, although significantly different product ratios and slower reaction times were observed. Importantly, the FeCz-NPs were found to be active as catalysts with the addition of 5-Cl-1-MeIm and H_2O_2 as oxidant in place of PFIB. In contrast, no catalytic activity is observed for the molecular species with H_2O_2 in the presence or absence of 5-Cl-1-MeIm. There is a strong dependence of the NP-mediated catalysis on the identity of the exogenous base. The catalytic activity of Fe^{III}Cz-NPs and H_2O_2 decreases dramatically with the series 5-Cl-1-MeIm > 1-MeIm ≫ Br-Im, pyridine. The origin of the effect of exogenous base, together with determining the mechanistic details of these NP-catalyzed reactions, merits further study.

Acknowledgment. We thank Dr. M. McCaffery of the Johns Hopkins University Integrated Imaging Center for

(44) Nam, W.; Oh, S. Y.; Sun, Y. J.; Kim, J.; Kim, W. K.; Woo, S. K.; Shin, W. *J. Org. Chem.* **2003**, *68*, 7903–7906.
(45) Nam, W.; Lee, H. J.; Oh, S. Y.; Kim, C.; Jang, H. G. *J. Inorg. Biochem.* **2000**, *80*, 219–225.
(46) Hermans, I.; Jacobs, P.; Peeters, J. *Chem.—Eur. J.* **2007**, *13*, 754–761.
(47) Agarwala, A.; Bandyopadhyay, D. *Catal. Lett.* **2008**, *124*, 256–261.

assistance with the TEM measurements. We are grateful to the NSF (CHE-0909587 to D.P.G. and CHE-0848786 to J.D.B.), and the Johns Hopkins University Institute for NanoBioTechnology (to D.P.G.) for funding. W.D.K. thanks the Camille and Henry Dreyfus Environmental Chemistry Postdoctoral Fellowship for financial support. S.R.L. is thankful for a Johns Hopkins University Provost Undergraduate Research Award. We thank Mr. B. Smith and Mr. Y. Ren for support with the DLS measurements, and Dr. H. Q. Mao for use of the DLS instrument. We also gratefully acknowledge input from C. M. Drain at Hunter College of CUNY for many insightful and useful discussions about this work.

Supporting Information Available: UV−vis data (Figures S1−S5), AFM image (Figure S6) and table of DLS data (Table S1). This material is available free of charge via the Internet at http://pubs.acs.org.